Published online 9 January 2009

Nucleic Acids Research, 2009, Vol. 37, No. 5 ***1463–1476***
doi:10.1093/nar/gkn1078

Insights into the architecture and stoichiometry of *Escherichia coli* PepA•DNA complexes involved in transcriptional control and site-specific DNA recombination by atomic force microscopy

Phu Nguyen Le Minh[1], Neel Devroede[1], Jan Massant[1], Dominique Maes[2] and Daniel Charlier[1,*]

[1]Erfelijkheidsleer en Microbiologie and [2]Laboratorium voor Ultrastructuur, Vrije Universiteit Brussel (VUB) and Vlaams Interuniversitair Instituut voor Biotechnologie (VIB), Pleinlaan 2, B-1050 Brussel, Belgium

Received August 4, 2008; Revised and Accepted December 23, 2008

ABSTRACT

Multifunctional Aminopeptidase A (PepA) from *Escherichia coli* is involved in the control of two distinct DNA transaction processes: transcriptional repression of the *carAB* operon, encoding carbamoyl phosphate synthase and site-specific resolution of ColE1-type plasmid multimers. Both processes require communication at a distance along a DNA molecule and PepA is the major structural component of the nucleoprotein complexes that underlie this communication. Atomic Force Microscopy was used to analyze the architecture of PepA·*carAB* and PepA·*cer* site complexes. Contour length measurements, bending angle analyses and volume determinations demonstrate that the *car*P1 operator is foreshortened by ~235 bp through wrapping around one PepA hexamer. The highly deformed part of the operator extends from slightly upstream of the –35 hexamer of the *car*P1 promoter to just downstream of the IHF-binding site, and comprises the binding sites for the PurR and RutR transcriptional regulators. This extreme remodeling of the *car*P1 control region provides a straightforward explanation for the strict requirement of PepA in the establishment of pyrimidine and purine-specific repression of *carAB* transcription. We further provide a direct physical proof that PepA is able to synapse two *cer* sites in direct repeat in a large interwrapped nucleoprotein complex, likely comprising two PepA hexamers.

INTRODUCTION

Aminopeptidase A (PepA) from *Escherichia coli* (E.C.3.4.11.10) is a multifunctional protein (1). It is a major aminopeptidase capable of digesting a broad range of peptides, with a preference for leucine or methionine as the N-terminal amino acid. Interestingly, PepA (alias XerB and CarP) turned out to be also a DNA-binding protein involved in two distinct cellular processes, site-specific DNA recombination (2,3) and transcriptional control (4). In both processes, the catalytic activity of PepA is not required (4,5).

PepA plays a crucial role in both pyrimidine and purine-specific repression of the upstream promoter P1 of the *carAB* operon encoding carbamoyl phosphate synthase (4,6,7). Binding of PepA upstream to the *car*P1 promoter of *E. coli* and *Salmonella typhimurium* protects two ~27-bp long stretches against DNase I digestion, but also induces a large number of regularly spaced hyperreactive sites, indicative of minor groove widening by DNA distortion (4,8) (Figure 1a). PepA is an essential element in the regulation of *car*P1 activity but integration host factor (IHF), PyrH (UMP-kinase), PurR (purine repressor) and RutR, recently identified as the regulator of pyrimidine utilization, are required as well for the full range modulation of promoter activity (7,9–11). Furthermore, PepA binds to the control region of its own gene, suggestive of negative autoregulation (4).

PepA is also required in the process of the monomerization of ColE1 and pSC101 plasmid multimers formed by homologous recombination. This reaction helps to ensure stable plasmid inheritance. PepA binds to the ColE1 *cer* and pSC101 *psi* sites, and in conjunction with ArgR (arginine repressor) and ArcA (anaerobic response regulator),

*To whom correspondence should be addressed. Tel: + 32 2 629 1342; Fax: + 32 2 629 1345; Email: dcharlie@vub.ac.be

respectively, ensures that the recombination is exclusively intramolecular (12–14). PepA and ArgR/ArcA bind to ~180-bp long accessory sequences adjacent to the 28–30-bp core site where the sequential strand exchange reactions are performed by the related XerC and XerD recombinases, members of the tyrosine family of recombinases (15). PepA and ArgR/ArcA are required to bring together two *cer*/*psi* sites in direct repeat in the multimer to form an interwrapped synaptic complex. PepA is clearly the major architectural element in this process; ArgR/ArcA stimulate the recombination reaction, but are dispensable *in vitro*, when the PepA concentration is sufficiently high (14,16). XerC and XerD also act at the *E. coli dif* site to resolve dimers of the chromosome; but in this case, recombination is controlled by the cell division protein FtsK (17).

The crystal structure of PepA (18) and mutant studies have provided some clues to the mode of action of this multifunctional protein that bears none of the well-characterized DNA-binding motives. The hexamer (6×55 kDa) is organized as a dimer of trimers (Figure 1c). Each subunit comprises a smaller N-terminal domain (residues 1–166) that is connected to a larger C-terminal domain (residues 193–503) through a long α-helix. The C-terminal domains cluster around the 3-fold axis and form the core of the enzyme. The catalytic site and the two metal-ion-binding sites are entirely comprised within this core. The N-terminal domains extend outwards to the corners of the triangle. They mediate interactions between the two trimers in the vicinity of the 2-fold axes and play an important role in DNA binding, as indicated by mutant studies (19,20). From the crystal structure and the charge distribution on the surface of hexameric PepA, it has also been proposed that a groove, running over the surface of the C-terminal core of the hexamer, would act as a DNA-binding groove (18). Mutant studies have corroborated this proposal (20).

Combined, these data strongly suggest that PepA acts in *carAB* regulation and site-specific DNA recombination as the major architectural protein that induces severe DNA deformations required for the elaboration of higher order nucleoprotein structures. However, the DNA-binding mode of PepA is unusual and not well characterized, and the molecular architecture of the regulatory and recombining complexes, including their stoichiometry is not yet solved. Here we use a single molecule approach to analyze PepA·DNA complexes formed with the *carAB* control region and the ColE1 *cer* site. Tapping mode atomic force microscopy (AFM) was used to unravel the architecture of these complexes. AFM allows the detection of DNA deformations such as bending, wrapping and spooling, quantification of the bending angle and DNA compaction, and in some instances the determination of the stoichiomety of protein·DNA complexes (21). Interestingly, the single-molecule approach also provides insights to the flexibility of protein·DNA complexes through the distribution of the bending angles and the degree of the DNA foreshortening. In recent years the technique has been applied in the study of several nucleoprotein complexes involved in transcription and transcription regulation and in other DNA transactions in both prokaryotes and eukaryotes (22,23).

MATERIALS AND METHODS

Overexpression and purification of PepA

PepA was purified from an IPTG-induced culture of *E. coli* strain JM101 transformed with the plasmid pKHW1, as described by Devroede *et al.* (24).

Preparation of DNA samples

The DNA molecules used in the AFM experiments were produced by PCR amplification using the ReadyMix TaqPCR reaction mix (Sigma-Aldrich). The 578-bp B1–B2 fragment was amplified with as template the plasmid pFW-carP1 + P2 (7) and the oligonucleotides AB1Bam (5′-GCGGGATCCGTTGAGTGGTAAGGA AAGCGG-3′) and AB2Eco (5′-CGGAATTCCTGGGT TCCGTCTTCCAGAAC-3′). The 642-bp fragment spanning the *carAB* control region was generated with the same template and the oligonucleotides AB1Bam and DC381r (5′-GCTTGGCTGCAGGTCGAAATTCG-3′). The 2050-bp 2*cer* fragment and the 1640-bp 1*cer* fragment were generated with plasmid pGIC009 (provided by B. Hallet) as a template and the pairs of oligonucleotides DC585f (5′-TACGCCAGCTGGCGAAAGGG-3′) plus DC586r (5′-GGTGTGTGGAATTGTGAGCG-3′), and DC585f plus DC607r (5′-TCTGCCTCGTGAAGAAG GTG-3′), as primers, respectively. pGIC009 was constructed starting from plasmid pKS493, containing a single *cer* site (13), according to the strategy utilized previously to construct pSDC134, a plasmid containing two *psi* sites in direct repeat (B. Hallet, personal communication). DNA fragments were purified by gel electrophoresis, excised and eluted using the GenElute gel extraction kit (Sigma-Aldrich). All oligonucleotides used in this work were purchased from Sigma Genosys.

Sample preparation for AFM

DNA molecules were diluted in binding buffer (10 mM Tris–HCl (pH 7.9), 125 mM KCl, 10 mM $MgCl_2$, 0.1 mM DTT, 25% glycerol) in a total volume of 15 µl. The diluted DNA was then mixed with an equal volume of adsorption buffer [40 mM Hepes (pH 6.87), 10 mM $NiCl_2 \cdot 6H_2O$] and 15 µl were deposited on freshly cleaved mica. After 5 min of adsorption, the samples were rinsed with deionized ultrapure water. Subsequently, excess water was blotted off with absorbing paper and finally the mica was blown dry in a stream of filtered air. PepA·DNA complexes were formed by incubating 25–35 ng of PepA with about 200 ng of DNA in the binding buffer in a total volume of 15 µl at 37°C for 20 min. Sample deposition was as described above for DNA molecules, allowing 3–5 min of adsorption.

Image acquisition and analysis

Images of 512×512 pixels were acquired with a NanoScope IIIa atomic force microscope (Digital Instruments/Veeco) operating in tapping mode at room temperature.

We used Nanoprobe SPM tips, type TESP (Veeco), with a 125 μm cantilever with a nominal spring constant of 50 N m^{-1} and resonance frequencies in the range from 279 to 362 kHz. The scan rate was 2 Hz and the scan size was 1.5 μm × 1.5 μm. All images used in one analysis were obtained with the same tip and deposition, and all the contour length and bending angle measurements were carried out with the same procedure. The NanoScope 6.11r1 software (Digital Instruments/Veeco) was used to flatten the images prior to analysis. Molecules were manually traced using ImageJ (25; available at rbs.info.nih.gov/ij/) to measure contour lengths and end-to-end distances. Contour length histograms were fitted to a normal distribution (Statistical Package for the Social Sciences). The persistence lengths (P) were calculated from the experimentally measured contour lengths (L) and the end-to-end distances (R) according to the formula: $<R^2>_{2D} = 4PL\ [1 - 2P/L(1 - e^{-L/2P})]$. Bending angle analysis was performed by applying the Bending Analysis Software (26; available at www.nat.vu.nl/compl/bendinganalysis). The bin sizes were chosen using the following formula as a guideline: optimal bin size is equal to the ratio of the range of measurements over the square root of the number of measurements. The apparent volume of the globular PepA·*carAB* operator complexed regions was calculated as follows: $V_{app} = \pi \times \text{height} \times (\text{width})^2/6$, assuming that the complexed regions have the shape of an oblate spheroid. The width was measured at a height of 0.5 nm as a correction for the height of the DNA molecule and the background. The apparent volume of the two-lobe PepA·2*cer* complexes were calculated as follows: $V_{app} = 3\pi abc/4$, with a, b and c the lengths of the semiaxes, assuming that they have an ellipsoidal shape. Volumes were also determined by the integration of the intensity of all the pixels composing the image, using a software developed for scanning probe microscopy (WSxM 4.0 Develop12.5 available at http://www.nanotec.es/wsxm_download.html). Both methods generated very similar data. Apparent volumes measured by AFM deviate significantly from the real volume and AFM images of soft biomolecules appear usually wider (because of tip convolution) and less high (because of interactions between the tip and the surface) than the sample itself. Therefore, only measurements from a single deposition and using the same tip can be used, and exclusively in a comparative manner. All calculated mean values are given with the standard deviation. The experimentally determined basepair rise for each fragment was systematically used to convert distances measured in nanometers into basepairs.

RESULTS

Visualization of bare DNA molecules

Four DNA fragments, two comprising the *carAB* operator, one carrying a single ColE1 *cer* site, and one carrying two *cer* sites in direct repeat were used for the analysis of PepA·DNA complexes (Figure 1). The 578-bp long B1–B2 fragment extends 428-bp upstream and 149-bp downstream of the *car*P1 transcription initiation site. It contains both promoters of the *carAB* operon and the binding sites for IHF, PepA, RutR, PurR and ArgR (Figure 1a). The B1-DC381 fragment of 642 bp has the same upstream border, but extends further downstream, into the vector sequence. The 2*cer* fragment of 2050 bp contains two copies of the *cer* site on 279-bp long direct repeats, separated by 1282 bp (Figure 1b). The 1*cer* fragment of 1640 bp has the same upstream border but is shorter and bears a single *cer* site only. Figure 2a and b shows some typical images of these unbound B1-DC381 and 2*cer* DNA fragments, respectively, deposited on mica and visualized by the tapping mode atomic force microscopy in air. The contour length (L) of the DNA molecules was measured by tracing along the length of the molecule from one end to the other using ImageJ (Figure 2). Only non-overlapping molecules were measured and visible anomalies were excluded from the analysis. The data were plotted in a histogram and a Gaussian fit was applied (Figure 2). The results for all four fragments are summarized in Table 1. All four sets of measurements resulted in a similar axial bp rise (0.31–0.33 nm/bp) that is slightly lower than the rise of canonical B-form DNA as determined by X-ray crystallography (0.34 nm/bp), but is in full agreement with basepair rise values determined in previous AFM studies. These small differences may be attributed to the smoothing procedure that rounds sharp bends and the limited resolution of the microscope, incapable of resolving bends with a small angle (27).

We also verified that the molecules were able to freely equilibrate on the mica surface, as in a 2D solution, and were not kinetically trapped on the surface without equilibration. The standard manner to distinguish between these two modes of deposition is to compare the values of experimentally obtained mean square end-to-end distances $\langle R^2\rangle_{exp}$ to the calculated mean square end-to-end distances of free equilibration $\langle R^2\rangle_{2D}$ and kinetic trapping $\langle R^2\rangle_{proj}$, based on the known contour lengths and assuming the standard value of 53 nm for the persistence length P of DNA molecules in solution (28). The persistence length P reflects the bendability of a DNA molecule and is a measure of the average length at which thermal energy causes a DNA molecule to bend in a different direction. For all four fragments, the experimentally determined $\langle R^2\rangle_{exp}$ values were consistent with the 2D model (Table 1). Furthermore, we have also included in the Table 1 the persistence length values calculated using the corresponding experimentally determined L and $\langle R^2\rangle$ values for each fragment, assuming that the molecules are at equilibrium in 2D. Independently, P was also determined for the two *carAB* fragments using the simulation-based bending analysis software developed by Dame *et al.* (26). The normalized R distribution of the molecules (R/L) was fitted using distributions obtained by simulations of DNA molecules exhibiting no protein-induced bending. The obtained L/P and P values were within the expected range for DNA (data not shown). Therefore, we may assume that free equilibration applied to all our sample analyses.

PepA binding induces a massive reduction of the *carAB* control region of ~235 bp

The images in Figure 3a and b show an overview AFM image and some typical PepA·DNA complexes formed

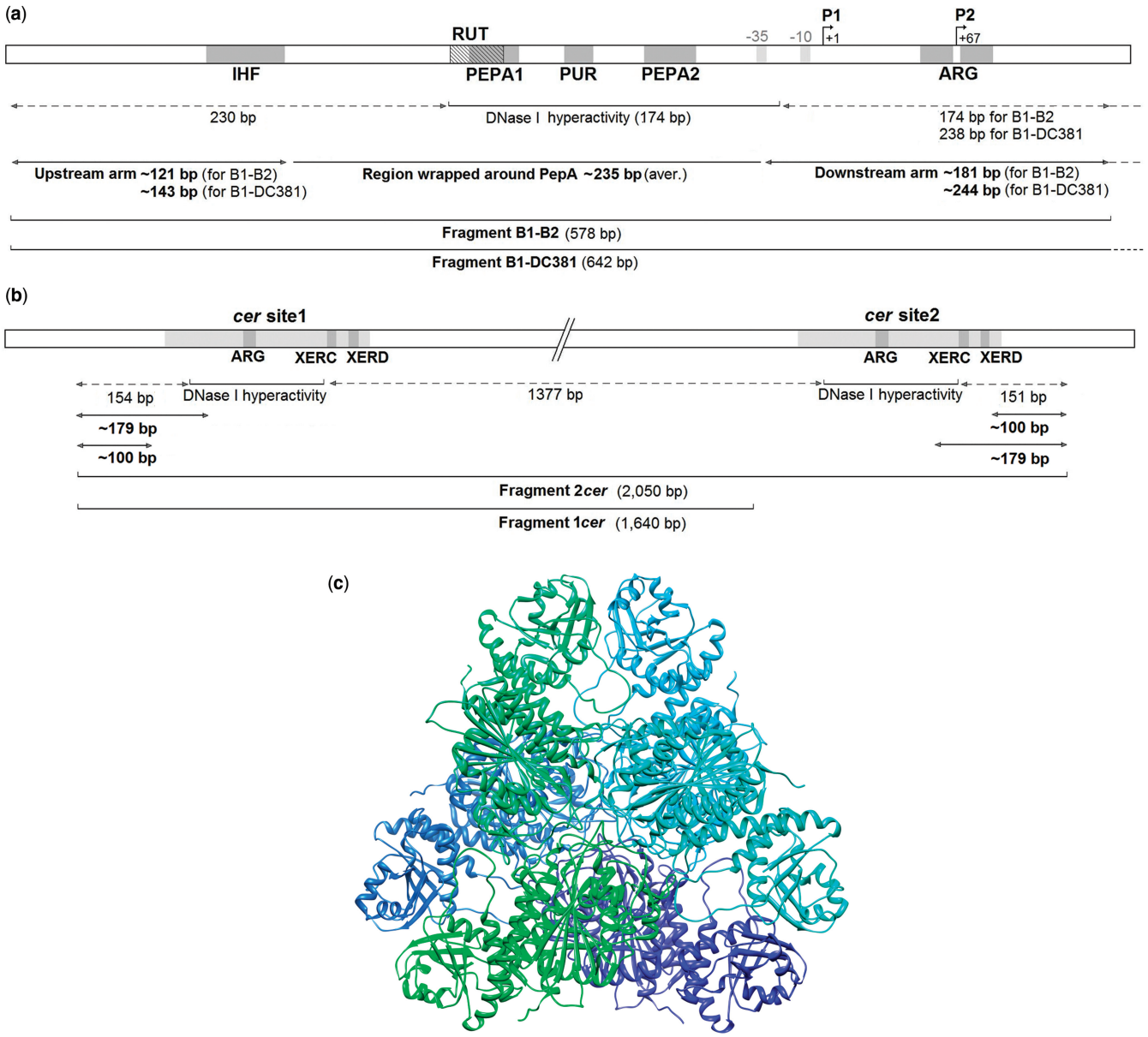

Figure 1. (**a**) Schematic view of the *carAB* control region showing the *car*P1 and *car*P2 promoters, the binding sites for the various regulatory and architectural proteins, and the size and the borders of the fragments used in the AFM study. PEPA1 and PEPA2 represent two continuous DNA stretches that are protected against DNase I digestion upon PepA binding; a line indicates the global zone showing alternating protection and regularly spaced sites hyperreactive for DNase I upon PepA binding (4). The length of the flanking regions, calculated on the basis of the footprints, is indicated with dotted lines. Similarly, we indicated the experimentally determined length of the arms and wrapped region (indicated in bold). The approximate length of the wrapped region is based on the average of different measurements (read-through and total visible contour length). (**b**) Organization of the two *cer* sites in direct repeat in plasmid pGIC009, and indication of the 2*cer* and 1*cer* fragments used in AFM studies. The binding sites for ArgR, XerC and XerD are boxed; a line represents the global zone exhibiting protection and hyperreactivity for DNase I upon PepA binding to a linear DNA fragment containing two *cer* sites in direct repeat; dotted lines indicate the predicted non-bound regions. Two alternatives for the arm lengths as determined by AFM are indicated (in bold) (3). (**c**) View along the 3-fold molecular axis of hexameric PepA, in which the two trimers are indicated in green and blue, respectively. The N-terminal domains point towards the corners of the triangle, the C-terminal domains cluster together at the center. Adapted from ref. (18).

with the *carAB* operator fragments, respectively. These complexes have a large, globular shaped structure and a sharp angle between the in- and outgoing DNA arms of the complexed region. Furthermore, the naked DNA part is visibly shortened as compared to the bare DNA molecules. These observations strongly suggest DNA wrapping. To analyze the DNA deformations induced by PepA more quantitatively, we measured the contour length of these molecules. The contour length of globular protein·DNA complexes can be measured in two manners: the 'visible length' and the 'read-through' length (Figure 3b). The visible contour length corresponds to the sum of the length of the two naked DNA arms; this might result in an underestimation of the length because of the 'shadow' of the protein causing a partial occlusion of the naked DNA (29). The read-through length corresponds to the contour

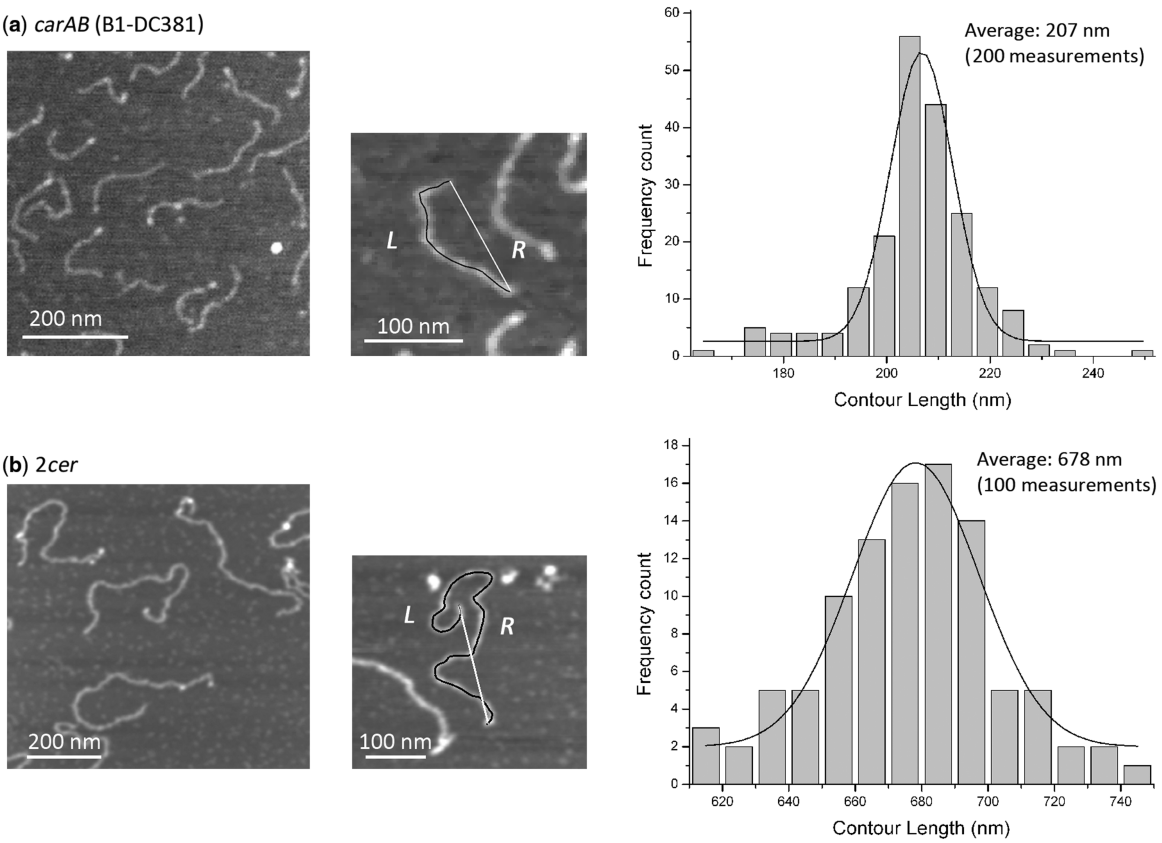

Figure 2. Overview AFM image of unbound B1-DC381 (**a**) and 2*cer* (**b**) DNA molecules, with indication of the contour length (*L*) and end-to-end distance (*R*), and a histogram of the contour length distribution of these molecules with an overlay of a normal distribution curve.

Table 1. DNA contour length of bare DNA fragments and derived axial bp rise and persistence length

Fragment name	Length (bp)	Number of fragments measured	Contour length in mm (SD)	Axial bp rise (nm/bp)	Average $<R^2>_{exp}$ [nm^2 SD]	Persistence length (nm)	Average $<R^2>_{2D}$ (nm^2)	Average $<R^2>_{proj}$ (nm^2)
B1–B2	578	477	181 (16.7)	0.31	17 700 (6100)	41	19 514	8986
B1–DC381	642	135	207 (12.3)	0.32	21 967 (7000)	42.4	24 600	10 958
2*cer*	2050	100	678 (26.6)	0.33	105 703 (78 800)	45	121344	44 180
1*cer*	1640	100	527 (18)	0.32	89 266 (56 500)	52.9	89 408	33 496

length measured along the naked DNA arms and the shortest path through the complexed region; this could result in an overestimation of the length of the naked DNA when the entry and exit points of the DNA arms are distant. The histograms with the distribution of the read-through and visible contour lengths for complexes formed with the 578-bp and the 642-bp *carAB* fragments are shown (Figure 3c–f). We measured the read-through contour length of 150 and 156 complexes formed with the 578-bp and 642-bp fragments, respectively. A Gaussian fit was applied and it yielded an average contour length of 107 nm (SD 18.2) for the 578-bp fragment and 137 nm (SD 17.5) for the 642-bp fragment (Table 2). This indicates that the binding of PepA to the *carAB* control region results in a massive apparent reduction of the contour length, ~74 and 70 nm, respectively, which corresponds to ~239 and 219 bp. The average total visible length of the complexes formed with the 578-bp and the 642-bp fragment was 94 nm (SD 15) and 125 nm (SD 13.2), respectively (Table 2), which indicates a foreshortening of the PepA-bound DNA by ~87 nm (~280 bp) and 83 nm (~259 bp). Taking into account that the read-through and visible length methods may lead to an under- and overestimation of the calculated foreshortening, respectively, we may reasonably estimate that PepA binding induces an apparent reduction in length of the *carAB* operator DNA of ~235 bp, likely by wrapping around a single PepA hexamer (see below). The length of the in- and outgoing arms of the complexes was plotted in a single histogram with a bimodal distribution that was fitted with two Gaussians. This resulted in two peaks corresponding to an average length of the individual arms of 37 nm (SD 8.5) (~121 bp) and 56 nm (SD 9.8) (181 bp) for the 578-bp fragment; 46 nm (SD 8.7) (~143 bp) and 78 nm (SD 9.7)

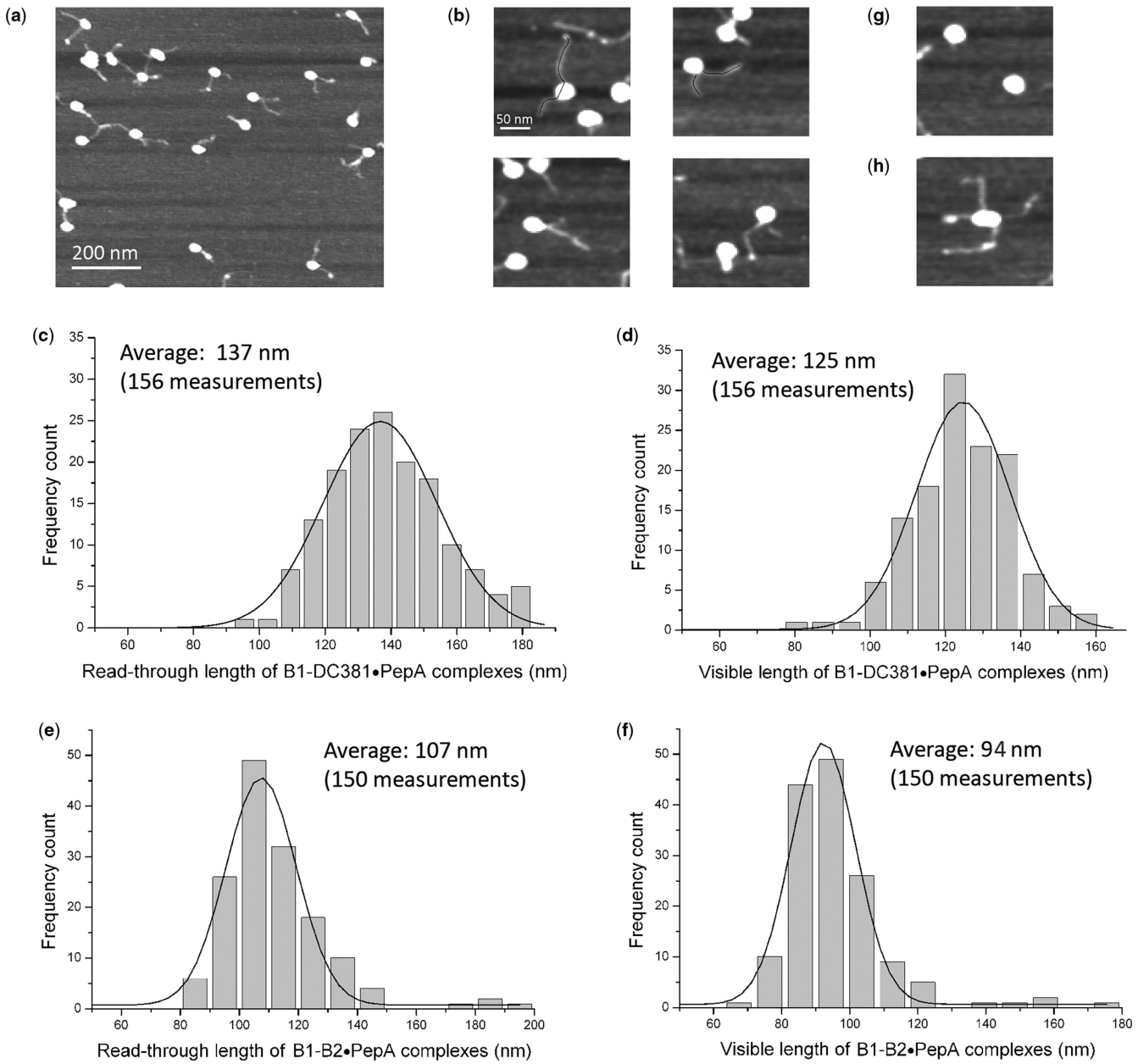

Figure 3. (**a**) Overview AFM image of PepA binding to the 642-bp *carAB* fragment B1-DC381. (**b**) Four examples of typical wrapped PepA·DNA complexes formed with the same *carAB* fragment, with indication of the read-through contour length and the visible contour length. (**c**, **d**) Histograms with an overlay of a normal distribution curve of the read-through and visible contour length, respectively, of 156 PepA·DNA complexes formed with the B1-DC381 fragment and of 150 complexes formed with the fragment B1–B2, shown in (**e**) and (**f**). (**g**) Unbound PepA molecules. (**h**) Example of a rare interwrapped χ-like complex comprising two DNA and two PepA molecules.

Table 2. Arms and contour lengths, and wrapping angle for *carAB*•PepA complexes

DNA–PepA complexes	Number of measurements	Length of short arm [nm (SD)]	Length of long arm [nm (SD)]	Visible contour length [nm (SD)]	Read-through contour length [nm (SD)]	Angle (bending analysis)
B1–B2	150	37.4 (8.5)	56.2 (9.8)	94 (15)	107.4 (18.2)	$120 \pm 10^{\circ}$
B1–DC381	156	46 (8.7)	78.2 (9.5)	124.7 (13.2)	136.8 (17.5)	$100 \pm 10^{\circ}$

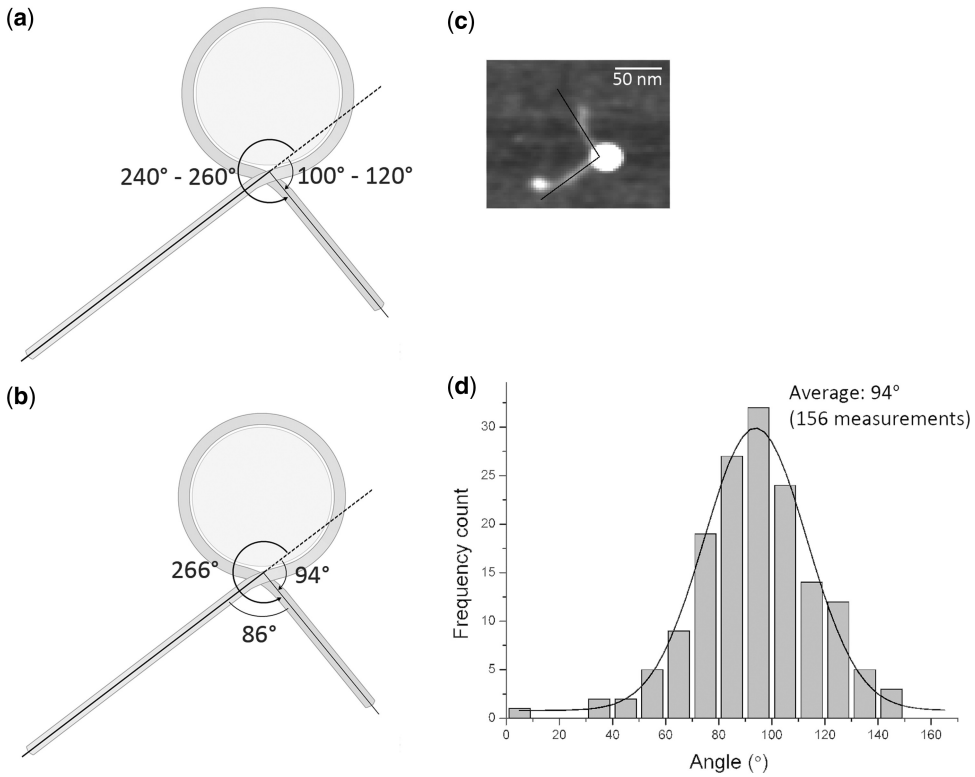

Figure 4. (**a**) Schematic presentation of a wrapped PepA·*carAB* complex showing the bending angles (100°–120°) obtained with complexes formed with the two *carAB* fragments as determined by the Bending Analysis Program using end-to-end distance measurements, and the corresponding calculated bending angles taking wrapping in the opposite orientation into account (240°–260°). (**b**) Schematic presentation of a wrapped PepA·*carAB* complex showing the measured angle of 86° between the in- and outgoing DNA arms (tangent method) of complexes formed with the B1-DC381 fragment, the calculated net apparent bending angle (94°) and the corresponding calculated bending angle assuming that the DNA is being wrapped in the opposite direction (266°). (**c**) AFM image of a globular PepA·DNA complex with indication of the angle between the in- and outgoing DNA arms as measured with the tangent method. (**d**) Histogram of the bending angle distribution obtained by the tangent method (180°—experimentally measured angle between in- and outgoing DNA arms), with an overlay of a normal distribution curve.

(~244 bp) for the 642-bp fragment (Table 2), indicating that the wrapped part of the operator extends approximately from positions –280 to –60, upstream of the start of *car*P1 transcription initiation (Figure 1a). The difference in length between the long arms of the complexes formed with the two DNA fragments corresponds almost precisely to the difference in length of the two fragments. Given that they share the same upstream border, we may conclude that the short arm of the complexes corresponds to the upstream part of the operator and the long arm to the downstream, promoter proximal part of the operator.

Besides these typical complexes, we observed unbound PepA molecules (Figure 3g) and a few χ-like structures with two short and two longer arms, protruding from a globular region with a two-lobe shape (Figure 3h). Most likely, these rare intermolecular structures were formed by protein–protein contact between two preformed PepA·*carAB* complexes, containing a single PepA hexamer each (see below for the stoichiometry of PepA·DNA complexes).

PepA induces wrapping of the *carAB* control region by ~260°

As mentioned above, the sharp angle between the in- and outgoing arms of the complexed regions suggest a pronounced bending or even wrapping. We applied a method developed by Dame *et al.* (26) that allows the analysis of bending angles based on the end-to-end distance (R) distribution of the complexes. The R distribution, normalized by $L(R/L)$, is fitted to histograms based on simulations using least squares minimization. The application of this method (Bending Analysis) indicated a best fit apparent bending angle of $120° \pm 10°$ for the set of complexes formed with the 578-bp fragment and of $100° \pm 10°$ for complexes formed with the 642-bp fragment. Taking into account the pronounced foreshortening of the complexed DNA molecules, this indicates that the *carAB* control region is being wrapped 240° to 260° in the opposite direction (Figure 4a), or 360° more if the DNA would make an additional turn around PepA (see Discussion section).

The apparent bending angle of complexes visualized by AFM can also be determined directly, by measuring the angle formed between the in- and outgoing DNA tails of the complexes (Figure 4b and c). The bending angle is then calculated by subtracting the measured angle from 180° (Figure 4b). This so-called 'tangent method' generally gives a rather broad distribution of bending angles that likely reflects the effects of thermal fluctuations and the flexibility of the complexes (27,30,31). The analysis of the PepA-bound 642-bp fragments resulted in an average apparent bending angle of 94° (SD 22.8) (Figure 4b–d),

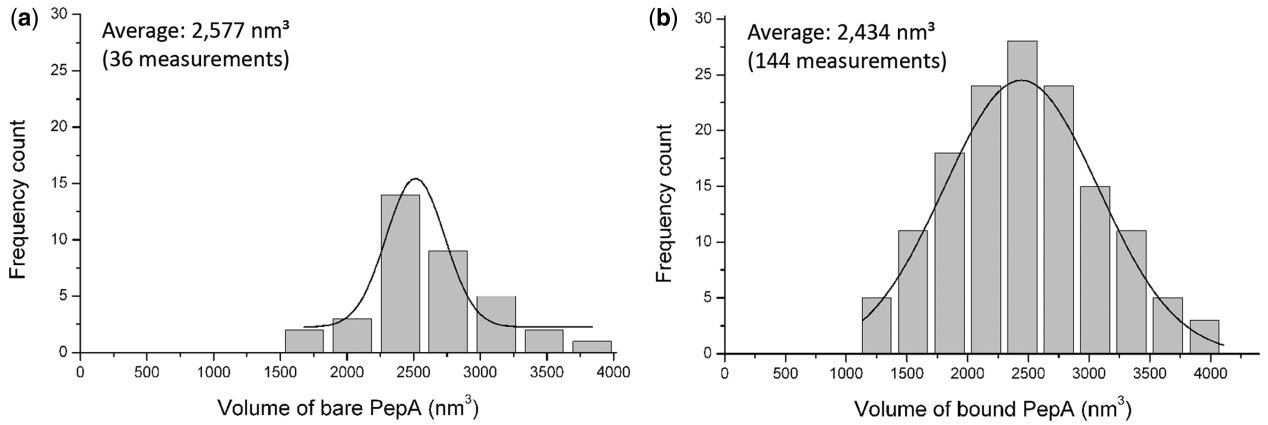

Figure 5. (**a** and **b**)Histograms of the volume analyses of unbound and DNA-bound (B1-DC381 fragment) PepA molecules, with an overlay of a normal distribution curve.

which is comparable to the 100° calculated for the same complexes with the method based on the distribution of end-to-end distances. Again, this would indicate that the DNA is being wrapped 266° in the opposite direction.

1:1 stoichiometry of PepA·*carAB* operator complexes

As neither the height nor the surface of a molecule measured by AFM are accurate, due to interactions between the tip and the surface, tip convolution and feedback settings, volume analyses by AFM have to be performed with molecules from a single deposition and measured with a single tip. Furthermore, the results can only be used in a comparative manner and have to be interpreted with caution. Taking these precautions into account, several authors were able to establish a relationship between the protein volume measured by AFM and the molecular mass of the protein (31–35). To determine the stoichiometry of the PepA·*carAB* operator complexes, we performed volume analyses on these complexes and on free hexameric PepA molecules (same deposition and tip). Both the free and the DNA-bound protein molecules have a similar and very regular appearance. Therefore, we calculated their volume assuming that they resemble an oblate spheroid (see Materials and methods section). From the distributions (Figure 5), we obtained an average apparent volume of 2434 nm^3 (SD 620) for DNA-bound PepA molecules (144 molecules analyzed), and 2577 nm^3 (SD 500) for the free PepA hexamers (36 molecules). Hence, both volumes are very similar and, therefore, we may conclude that a single PepA hexamer binds to the *carAB* control region and wraps ~235 bp of the operator. At first sight, it may seem surprising that wrapped DNA does not lead to a significant increase in the volume of bound PepA molecules, but this was previously observed with the archaeal transcriptional regulator Ss-LrpB (31) that wraps about 100 bp. Apart from the limitations of the technique already mentioned above, additional factors such as docking of DNA stretches into grooves on the surface of the protein, might contribute to the observed absence of increase in volume upon significant increase in mass.

PepA induces wrapping and looping-out with two *cer* sites in direct repeat

Binding of PepA to the 2050-bp 2*cer* fragment resulted in the formation of different classes of complexes with a distinct shape (Figure 6). The simple 'linear' types, showing one or two globular regions, likely represent molecules with respectively one and two *cer* sites bound by individual PepA hexamers (Figure 6a). Most interestingly, however, are the complexes exhibiting a large DNA loop, that could be observed consistently with the 2*cer* fragment, and only with the 2*cer* fragment (see below). They constitute about two-third of the non-entangled PepA-bound molecules. These complexes likely represent single DNA molecules in which the two *cer* sites in direct repeat are brought together in an interwrapped synaptic complex. A gallery of such complexes is shown in Figure 6b (flattened presentation) and Figure 6c (tilted surface plots to emphasize the topography). They consist of a prominent globular region, with an irregular and apparently two-lobe shape (see also below: stoichiometry of PepA·2*cer* complexes), from which protrude a DNA loop of constant size, and two short asymmetric in- and outgoing DNA arms that exit the globular complex on opposite sides. The two arms were not always discernible; in many instances one arm was not visible, likely due to the particular orientation of these molecules on the mica surface, and the bulkiness of the globular region. The contour length of the loop from 60 PepA·2*cer* complexes was measured. The data plotted in Figure 6d resulted in an average loop length of 310 nm (SD 44.1), which corresponds to ~942 bp. The average contour length of the longest arm was 59 nm (SD 15.0) or ~179 bp, whereas the shortest arm was 33 nm (SD 7.1) or ~100 bp long (Figure 6e). However, since the position of the two *cer* sites with respect to the limits of the fragment is very similar, we cannot assign a particular arm length to the upstream or downstream border of the fragment (Figure 1b). Therefore, the two alternatives are indicated in Figure 1b. Altogether this results in a total visible length of 403 nm or ~1221 bp, which in turn indicates an impressive apparent reduction of the DNA contour length (~275 nm or 833 bp).

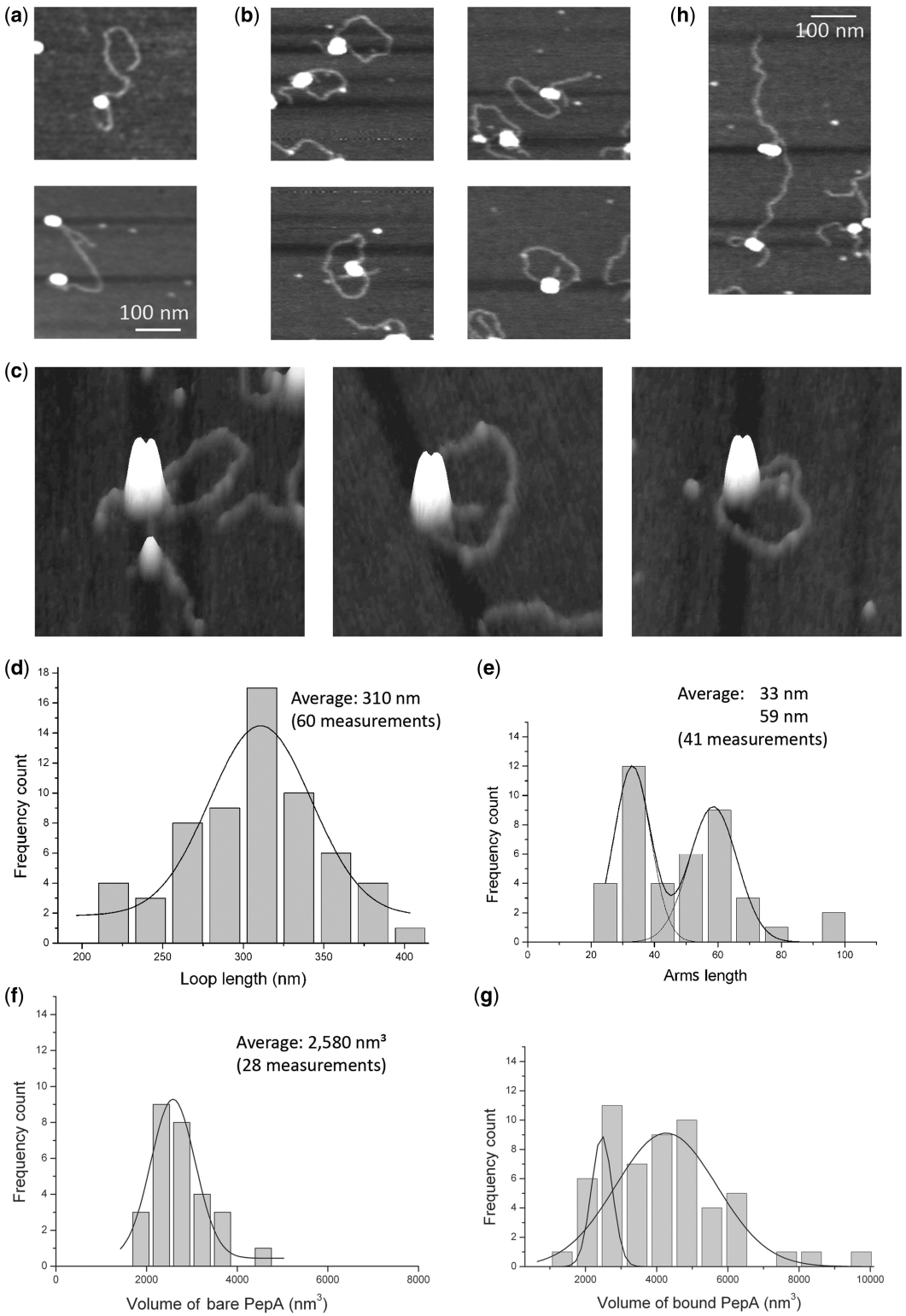

Figure 6. (**a**) AFM images of two linear 2*cer* DNA fragments with one and two complexed regions, respectively. (**b**) Gallery of AFM images of PepA·2*cer* complexes showing a DNA loop and a single complexed region with a two-lobe shape, from which protrude the DNA arms. (**c**) AFM images of three similar PepA·2*cer* complexes presented as surface plots at a 15° viewing angle to emphasize the topography. (**d**) Histogram of the contour length of the DNA loop formed by bringing together the two *cer* sites in a wrapped nucleoprotein complex with a two-lobe shape. (**e**) Histogram of lengths of protruding arms from the globular complexed region showing two peaks, at 33 nm and 59 nm. (**f**) Histogram of the volume analysis of unbound PepA with an overlay of a normal distribution curve. (**g**) Histogram of volume measurements of looped 2*cer* DNA·PepA complexes, showing a bi-modal distribution. (**h**) AFM image of two 2*cer* DNA fragments held together by PepA.

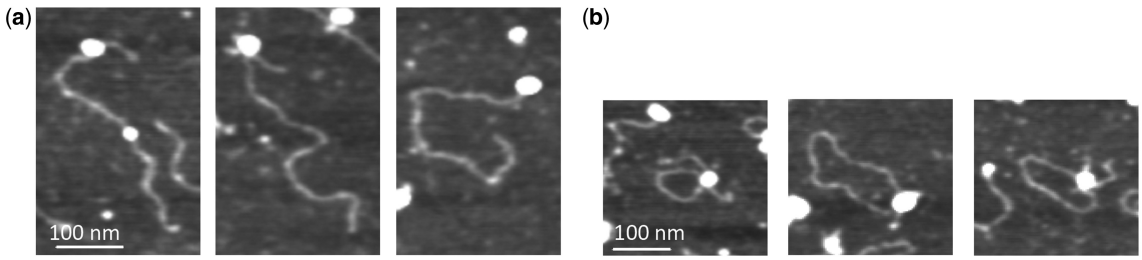

Figure 7. (**a**) Three AFM images of 1*cer*·PepA complexes with a linear shape. (**b**) Three AFM images of 1*cer*·PepA complexes showing a DNA loop of variable size.

Furthermore, we could observe some rare structures that are longer than the unit length of the 2*cer* fragment and are apparently composed of two DNA molecules held together by two PepA hexamers (Figure 6h). Structurally they resemble the intermolecular χ-like structure described above for the *carAB* fragment, but the short arm is not necessarily visible.

Interwrapped synaptic *cer* complexes contain two PepA hexamers

A visual inspection of PepA-bound 2*cer* fragments showing a DNA loop (Figure 6b and c) indicates that most of the complexed regions do not show the smooth and regular appearance of the globular PepA·*carAB* operator complexes, but instead have an irregular, two-lobe shape, clearly different from the unbound and single site-bound PepA molecules (Figure 6c), suggesting that they may contain two PepA hexamers. We measured the height and the short and long axis of these ellipsoidal structures and calculated their volume (see Materials and methods section). For the free PepA hexamer (28 molecules, determined from the same deposition), we obtained an average apparent volume of 2580 nm^3 (SD 605) (Figure 6f). The histogram of looped DNA-bound PepA molecules suggests a bimodal distribution (Figure 6g). Non-linear least-square fitting of the cumulative density function with two Gaussians (data not shown) indeed results in two normal distributions, one with an amplitude of 0.17 and a mean of 2820 nm^3, and the second one with an amplitude of 0.83 and a mean of 4230 nm^3. This indicates that 17% of the complexes have a volume close to that of a single PepA hexamer. They likely represent DNA molecules bound at one *cer* site only, forming an apparent loop by random DNA crossing, as also observed with the 1*cer* fragment (see below). In contrast, 83% of the complexes show a significantly higher volume, almost double that of a free PepA molecule, suggesting the binding of two PepA hexamers. Furthermore, the volume analysis of a limited set of linear 2*cer*·PepA complexes (25 molecules) indicated an average volume of 2291 nm^3 (SD 944). Volume analysis based on the integration of the intensity of pixels pointed to the same conclusions (data not shown). Hence, both the shape and the apparent volume analyses strongly suggest that two PepA hexamers are required to assemble a pair of *cer* sites in direct repeat into an interwrapped synaptic complex.

PepA binding to a single *cer* site shortens the DNA contour length with ~210 bp

To further assess the specificity of the looped complexes formed with the 2*cer* fragment, we analyzed PepA·DNA complexes formed with the 1640-bp 1*cer* fragment. Some typical complexes with a single globular region are shown in Figure 7a. The average read-through contour length of these molecules was 460 nm (SD 16.2) or ~1438 bp, which indicates a PepA-induced reduction of the contour length of 67 nm (~209 bp), which is strikingly similar to the PepA-induced foreshortening of the *carAB* control region (~235 bp), and suggests a similar structure for the PepA·*carAB* and PepA·1*cer* nucleoprotein complexes. The volume of these complexes (1921 nm^3, SD 845; 24 molecules analyzed) is also very similar to that of the *carAB*·PepA complexes and significantly lower than that of the looped 2*cer*·PepA complexes. Occasionally, some looped molecules could also be observed with the 1*cer* fragment (Figure 7b). However, contour length measurements indicated that these loops are extremely variable in size and cannot be fitted in a Gaussian distribution (data not shown). Therefore, it can be concluded that these loops were generated randomly during the deposition process, and not by the binding of PepA to two specific sites on the DNA.

DISCUSSION

Guided and controlled communication at a distance along a single DNA or RNA molecule or among different molecules is an important element in numerous essential biological processes such as replication, repair, packing, packaging, transfer and recombination of DNA (homologous, site-specific, transposition, V(D)J reshuffling involved in antibody production), transcriptional regulation, pre-mRNA splicing and translation. *E. coli* PepA is absolutely required to establish a selective long distance communication in two distinct processes, transcriptional regulation and site-specific DNA recombination. In the control of *carAB* expression PepA-induced remodelling of the control region is required to ensure the cross-talk between various upstream bound transcription regulators and the RNA polymerase; in the resolution of ColE1 type plasmids PepA works as a 'topological filter' that imposes the resolution selectivity on the recombination reaction.

Regulatory PepA·*carAB* operator complexes

Overall we show that the binding of a single PepA hexamer to the *carAB* control region results in the wrapping of ~235 bp of the *car*P1 operator. In contrast, the other regulatory and architectural elements, ArgR, PurR, RutR and IHF, that bind to the *carAB* control region (Figure 1a) bend the operator DNA considerably, but without significant DNA condensation (7; unpublished observations from this laboratory). The PepA-induced foreshortening is huge in comparison to the amount of DNA that is condensed in several other prokaryotic transcriptional or regulatory complexes, but more similar to the nucleosomal DNA (~150 bp) that is wound ~1.65 times around the octameric histone core (~110 kDa) (~200 bp including the linker histone H1). For instance, *E. coli* RNA polymerase (~460 kDa) and some smaller bacterial and archaeal Lrp-like transcriptional regulators wrap about 100 bp only (27,30,31,36). Molecular modeling by Reijns *et al.* (20) indicates that about ~70 bp could occupy a single C-terminal groove and its two flanking N-terminal DNA-binding sites. Based on the triangular shape of the hexameric PepA crystal structure with an edge length of about ~135 Å and a thickness of ~80 Å, a minimum of 49 nm (144 bp) of DNA would be required to make a single tight wrap. This is considerably shorter than the ~235-bp foreshortening of the *carAB* operator by wrapping around a single PepA hexamer. Yet, it appears unlikely that the operator would make two full turns around PepA. Rather, we propose the existence of regions of tight interactions (N-terminal binding sites and C-terminal grooves) connected by loops that are in loose contacts, containing the binding sites for various transcriptional regulators involved in *carAB* regulation. Such architecture is quite different from the nucleosome structure where about 140 hydrogen bonds provide the driving force for the tight and regular wrapping of the DNA around the octameric histone core.

Why does *carAB* regulation rely on such a pronounced remodeling of the operator region? Possibly, the rationale for this mechanism is to be found in the multitude of transcriptional regulators involved in the modulation of *car*P1 promoter activity. There is evidently not enough space to bind all these proteins in the immediate vicinity of the RNA polymerase binding site, unless the various binding sites would largely overlap, which might create a problem of binding specificity. Furthermore, the promoter region must also integrate a TTT stretch involved in uracil-sensitive reiterative transcription initiation control (stuttering) (37), and a discriminator box involved in stringent control (38).

Previously we have shown that the binding of PepA to the *carAB* control region of *E. coli* and *S. typhimurium* induces a large number of regularly spaced sites hyperreactive for DNase I spreading over nearly 200 bp (4,8). This zone is almost completely comprised within the wrapped part of the operator as determined in this work by AFM imaging of PepA·*carAB* operator complexes. The downstream borders determined by the two techniques coincide very well, whereas the upstream border of the wrapped region extends farther upstream in the AFM technique (Figure 1a). The entire *carAB* control region is extremely A + T rich and contains numerous stretches of four or more consecutive A or T residues. When aligned in phase with the periodicity of the DNA helix, such stretches impose an intrinsic bending of the DNA which in turn would reduce the energetic cost for the pronounced PepA-induced deformations of this region.

Based on our AFM imaging, DNase I footprinting and PepA mutant studies, we propose a model for PepA-induced wrapping of the *carAB* control region that is based on one of the models previously proposed for the formation of the synaptic complex involved in *cer*/Xer recombination (20; see also below). In this model two DNA stretches directly interact with two of the three composite binding zones present on the PepA hexamer. Each DNA binding path is composed of a C-terminal groove segment and the corresponding N-terminal edges of the triangular PepA structure (Figure 8a). The third path would not be contacted since the groove and the DNA run in opposite directions. In this model, the intervening DNA, comprising the PUR box is looped out (Figure 8a). This looping is at least compatible with the occurrence of PepA induced hyperreactive for DNase I in the PUR box and the immediate flanking sequences. The simultaneous binding of PepA and PurR has to be guaranteed since *in vivo* and *in vitro* experiments indicated that the PurR-dependent repression of P1 activity is completely abolished in a *pepA* mutant, and that activated PurR is unable to repress P1 activity in a single round *in vitro* transcription system containing purified PurR and RNA polymerase but no PepA (7,24). Therefore, PurR relies on PepA to exert its regulatory effect and the PepA-dependent remodeling of the operator appears to be required to bring PurR in the vicinity of the RNA polymerase. Notice that a similar situation prevails for the binding of ArgR and ArcA to the *cer* and *psi* sites of the ColE1 and pSC101 plasmids, respectively. The position of the binding site for these regulators implies that ArgR and ArcA should also be able to bind the plectonemic interwrapped PepA·DNA complexes (Figure 1b). ArgR and ArcA are required *in vivo*, and *in vitro* they stimulate the recombination reaction.

In contrast, it was recently suggested but not proven, that the binding of the novel RutR regulator, far upstream of the P1 promoter (Figure 1a), would inhibit the binding of PepA (11). RutR (b1013) belongs to the TetR family of transcriptional regulators and was shown to stimulate *car*P1 activity in a uracil-sensitive manner (11). However, the pyrimidine-specific regulation of *car*P1 can not only be governed by an antagonistic binding of RutR and PepA. *In vivo* assays indicate that pyrimidine-dependent modulation of *car*P1 activity is reduced but not abolished in a $\triangle rutR$ mutant (11; unpublished observations from this laboratory) and, furthermore, UMP kinase, the essential *pyrH* product, is involved in the control of *car*P1 activity as well (10). Binding of PyrH to the *carAB* operator DNA has not been demonstrated, but mutant studies and the local charge distribution on the surface of the PepA and PyrH hexamers suggest the possibility of recruitment of PyrH by protein–protein contacts (10,19,39,40).

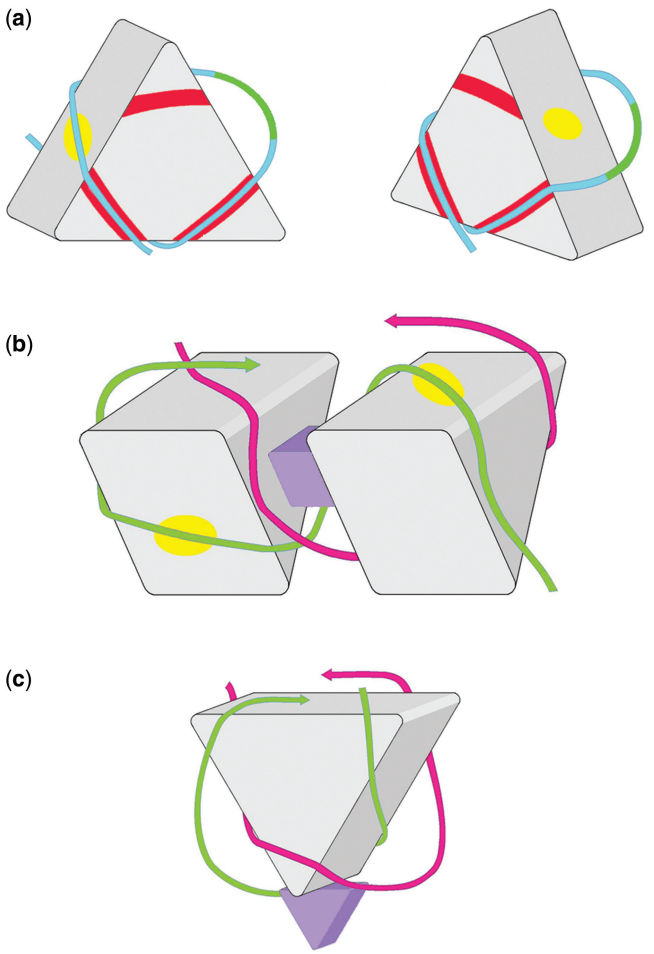

Figure 8. Cartoon presentation of PepA·DNA complexes. (**a**) Front and side view of a nucleoprotein complex with the *carAB* control region wrapped around a single PepA hexamer. In this model the operator DNA contacts two C-terminal groove segments (colored in yellow) and the adjacent N-terminal DNA binding paths (in red, at the edges of the triangle). The third groove segment is not contacted and runs in a direction opposite to that of the overlying DNA, comprising the PurR binding site (colored in green). (**b**) Modified Sträter model for the interwrapped synaptic PepA·*cer* site recombination complex as presented previously by Reijns *et al.* (20). In this model, two *cer* sites and the flanking region (colored in green and magenta) are brought together by two PepA hexamers. The DNA is wrapped and contacts the PepA hexamers in such a manner that each *cer* site contacts one C-terminal-groove and the adjacent N-terminal DNA-binding paths on each PepA hexamer. In this cartoon a single hexameric ArgR molecule (purple triangle) is sandwiched between the two PepA hexamers. (**c**) Model with a different stoichiometry proposed by Reijns *et al.* (20) for the interwrapped *cer* synaptic complex in which two *cer* sites are brought together in a nucleoprotein complex containing a single PepA hexamer. Two crossings of the DNA are trapped on two of the three faces of the hexameric PepA triangle. A single hexameric ArgR molecule might contribute to the stabilization of the bend.

These protein–protein contacts would distinguish the mode of action of PepA in transcriptional control from its role in site-specific DNA recombination. In this context it is worth noticing that different selection strategies have provided single amino-acid substitution mutants of *pepA* that are still proficient for ColE1 dimer resolution, but deficient in transcriptional control (19,20). The corresponding proteins still bind the *carAB* control region and the *cer* site, but are unable to repress *car*P1 activity. Furthermore, hybrid PepA proteins bearing parts of the homologous protein from *Pseudomonas aeruginosa* or *Haemophilus influenza* were able to complement an *E. coli pepA* knock-out mutant for the resolution reaction, but not for *carAB* regulation (20). Therefore, there is definitely more to the role of PepA in transcriptional control than simply DNA binding and remodeling of the operator DNA, even though this is clearly a crucial element for the elaboration of the higher order structures required for both the purine and pyrimidine-specific regulation. Further work is required to unravel all the protein–protein and protein–DNA cross-talks and the detailed architecture of the corresponding complexes involved in *carAB* regulation.

Stoichiometry and models of synaptic PepA·*cer* complexes

Like many other DNA recombination reactions, XerCD recombination at *cer in vivo* shows an absolute requirement for *trans*- and *cis*-acting accessory elements (12). These accessory but essential elements promote the formation of a specific topological complex that imposes constraints on the recombination reaction catalyzed by XerCD, ensuring that only directly repeated sites on a plasmid dimer will be recombined efficiently. Other recombination reactions catalyzed by serine and tyrosine recombinases use small DNA-binding proteins (such as IHF or FIS), additional but catalytically inactive copies of the recombinase molecules, and/or the geometry of the complex to sense the topology of the DNA and to enhance the reaction rate (41 and references therein).

Several models, with a different stoichiometry have been proposed for the synaptic *cer* complex (18,20). The most recent models, based on the identification of the DNA-binding path as identified by *pepA* mutant studies propose: (i) an adaptation of the Sträter model that contains two PepA hexamers and (ii) a novel model in which two *cer* sites are wrapped around a single PepA hexamer (20) (Figure 8b and c). In the adapted Sträter model (Figure 8b), each *cer* site interacts with the N-terminal DNA-binding paths and passes through two C-terminal grooves, one on each PepA hexamer. Thus, the two sites wrap around each other just enough to form an antiparallel synaptic complex and to account for the product topology of XerCD recombination, a 4-node catenane. In the novel model with a different stoichiometry (Figure 8c), two plectonemic DNA crossings are trapped on two faces of a single triangular PepA hexamer, whereas the third face would be occupied by the heterotetrameric XerCD recombinase. Even though the latter model has the preference of the authors in the Reijns paper (20), both models are largely consistent with the published footprints (3) and could not yet be discerned in the absence of data on the stoichiometry of the synaptic complex (20). Although the volume measurement by AFM have to be interpreted with caution, both the shape and the volume of the PepA·*cer* complexes suggest the presence of two PepA hexamers in the interwrapped synaptic complexes. Indeed, linear complexes formed with the 2*cer* and 1*cer* fragment do not show the bi-lobe shape and have a

significantly lower volume than that of the looped structure, close to that of a free hexameric PepA molecule. Therefore, our data corroborate the adapted Sträter model (Figure 8b) rather than the single PepA hexamer model (Figure 8c). Furthermore, and even though the measurements of free DNA parts may lead to an underestimation of the non-bound regions, the impressive foreshortening of the DNA in the PepA·2*cer* complexes (~800 bp) also indicates a complex path for the DNA in the synaptic complex that is more compatible with the wrapping around two PepA hexamers, rather than one. The adapted Sträter model depicted in Figure 8b shows one ArgR hexamer sandwiched in between two PepA hexamers. Our results and previous mutant studies (20) indicate that two complexed regions may assemble in the absence of ArgR, by protein–protein contact between two PepA molecules, as observed in the χ-like structures, or much more stably, by the interwrapping of two DNA segments around two PepA hexamers, possibly accompanied by protein–protein contacts, as in the looped PepA·2*cer* structures. Therefore, ArgR does not appear to be absolutely required for the formation of the synaptic complex.

The formation of a synaptic complex with PepA binding to two *cer* sites in direct repeat on a linear DNA fragment as demonstrated here does not automatically imply that this complex would be a good substrate for XerCD-mediated recombination. Indeed supercoiling appears to be a supplementary requirement for efficient dimer resolution (13).

ACKNOWLEDGEMENTS

We thank Dr ir. Ronnie Willaert for assistance with the atomic force microscope, and Dr B. Hallet for the gift of plasmid pGIC009. Many thanks again to Dr B. Hallet and Dr ir. Eveline Peeters for valuable suggestions and critical reading of the manuscript. We also thank the reviewers for their helpful remarks and suggestions.

FUNDING

Research-Foundation-Flanders (FWO-Vlaanderen G.044.02, G.0429.06), Reseach Council of the Brussels University (OZR835), Flanders Interuniversity Institute for Biotechnology (VIB), Vlaamse Gemeenschapscommissie. Research-Foundation-Flanders (to J.M.). Funding for open access charge: Research Foundation Flanders (FWO-Vlaanderen G.0429.06).

Conflict of interest statement. None declared.

REFERENCES

1. Colloms,S.D. (2003) Leucyl aminopeptidase A. In Barrett,A.J., Rawlings,N.D. and Woessner,J.F. (eds), *Handbook of Proteolytic Enzymes*, 2nd edn., Academic Press, Washington, DC.
2. Stirling,C.J., Colloms,S.D., Collins,J.F., Szatmari,G. and Sherratt,D.J. (1989) *xerB*, an *Escherichia coli* gene required for plasmid ColE1 site-specific recombination, is identical to *pepA*, encoding aminopeptidase A, a protein with substantial similarity to bovine lens leucine aminopeptidase. *EMBO J.*, **8**, 1623–1627.
3. Alén,C., Sherratt,D.J. and Colloms,S.D. (1997) Direct interaction of aminopeptidase A with recombination site DNA in Xer site-specific recombination. *EMBO J.*, **16**, 5188–5197.
4. Charlier,D., Hassanzadeh,G., Kholti,A., Gigot,D., Piérard,A. and Glansdorff,N. (1995) *carP*, involved in pyrimidine regulation of the *Escherichia coli* carbamoylphosphate synthetase operon encodes a sequence-specific DNA-binding protein identical to XerB and PepA, also required for resolution of ColE1 multimers. *J. Mol. Biol.*, **250**, 392–406.
5. McCulloch,R., Burke,M.E. and Sherratt,D. (1994) Peptidase activity of *Escherichia coli* aminopeptidase A is not required for its role in Xer site-specific recombination. *Mol. Microbiol.*, **12**, 241–251.
6. Roovers,M., Charlier,D., Feller,A., Gigot,D., Holemans,F., Lissens,W., Piérard,A. and Glansdorff,N. (1988) *carP*, a novel gene regulating the transcription of the carbamoylhosphate synthetase operon of *Escherichia coli*. *J. Mol. Biol.*, **204**, 857–865.
7. Devroede,N., Thia-Toong,T.-L., Gigot,D., Maes,D. and Charlier,D. (2004) Purine and pyrimidine-specific repression of the *Escherichia coli carAB* operon are functionally and structurally coupled. *J. Mol. Biol.*, **336**, 25–42.
8. Charlier,D., Gigot,D., Huysveld,N., Roovers,M., Piérard,A. and Glansdorff,N. (1995) Pyrimidine regulation of the *Escherichia coli* and *Salmonella typhimurium carAB* operons: CarP and integration host factor (IHF) modulate the methylation status of a GATC site present in the control region. *J. Mol. Biol.*, **250**, 383–391.
9. Charlier,D., Roovers,M., Gigot,D., Huysveld,N., Piérard,A. and Glansdorff,N. (1993) Integration host factor (IHF) modulates the expression of the pyrimidine-specific promoter of the *carAB* operons of *Escherichia coli* K12 and *Salmonella typhimurium* LT2. *Mol. Gen. Genet.*, **237**, 273–286.
10. Kholti,A., Charlier,D., Gigot,D., Huysveld,N. and Glansdorff,N. (1998) *pyrH*-encoded UMP-kinase directly participates in pyrimidine-specific modulation of promoter activity in *Escherichia coli*. *J. Mol. Biol.*, **280**, 571–582.
11. Shimada,T., Hirao,K., Kori,A., Yamamoto,K. and Ishihama,A. (2007) RutR is the uracil/thymine-sensing master regulator of a set of genes for synthesis and degradation of pyrimidines. *Mol. Mocrobiol.*, **66**, 744–757.
12. Guhathakurta,A., Viney,I. and Summers,D. (1996) Accessory proteins impose site selectivity during ColE1 dimer resolution. *Mol. Microbiol.*, **20**, 613–620.
13. Colloms,S.D., McCulloch,R., Grant,K., Neilson,L. and Sherratt,D.J. (1996) Xer-mediated site-specific recombination *in vitro*. *EMBO J.*, **15**, 1172–1181.
14. Colloms,S.D., Alén,C. and Sherratt,D.J. (1998) The ArcA/ArcB two-component regulatory system of *Escherichia coli* is essential for Xer site-specific recombination at *psi*. *Mol. Microbiol.*, **28**, 521–530.
15. Blakely,G., May,G., McCulloch,R., Arciszewska,L., Burke,M., Lovett,S. and Sherratt,D.J. (1993) Two related recombinases are required for site-specific recombination at *dif* and *cer* in *E. coli* K12. *Cell*, **75**, 351–361.
16. Gourlay,S.C. and Colloms,S.D. (2004) Control of Cre recombination by regulatory elements from Xer recombination systems. *Mol. Microbiol.*, **52**, 53–65.
17. Aussel,L., Barre,F.X., Aroyo,M., Stasiak,A.Z. and Sherrat,D.J. (2002) FtsK is a DNA motor protein that activates chromosome dimer resolution by switching the catalytic state of the XerC and XerD recombinases. *Cell*, **108**, 195–205.
18. Sträter,N., Sherratt,D.J. and Colloms,S.D. (1999) X-ray structure of aminopeptidase A from *Escherichia coli* and a model for the nucleoprotein complex in Xer site-specific recombination. *EMBO J.*, **18**, 4513–4522.
19. Charlier,D., Kholti,A., Huysveld,N., Gigot,D., Maes,D., Thia-Toong,T.-L. and Glansdorff,N. (2000) Mutational analysis of *Escherichia coli* PepA, a multifunctional DNA-binding aminopeptidase. *J. Mol. Biol.*, **302**, 411–426.
20. Reijns,M., Lu,Y., Leach,S. and Colloms,S.D. (2005) Mutagenesis of PepA suggests a new model for the Xer/*cer* synaptic complex. *Mol. Microbiol.*, **57**, 927–941.
21. Yang,Y., Wang,H. and Erie,D. (2002) Quantitative characterization of biomolecular assemblies and interactions using atomic force microscopy. *Methods*, **29**, 175–187.

22. Dame,R.T., Wyman,C. and Goosen,N. (2003) Insights into the regulation of transcription by scanning force microscopy. *J. Microsc.*, **212**, 244–253.
23. Cellai,S., Mangiarotti,L., Vannini,N., Naryshkin,N., Kortkhonjia,E., Ebright,R.H. and Rivetti,C. (2007) Upstream promoter sequences and αCTD mediate stable DNA wrapping within the RNA polymerase-promoter complex. *EMBO reports*, **8**, 271–278.
24. Devroede,N., Huysveld,N. and Charlier,D. (2006) Mutational analysis of intervening sequences connecting the binding sites for integration host factor, PepA, PurR, and RNA polymerase in the control region of the *Escherichia coli carAB* operon, encoding carbamoylphosphate synthase. *J. Bacteriol.*, **188**, 3236–3245.
25. Abramoff,M.D., Magelhaes,P.J. and Ram,S.J. (2004) Image processing with ImageJ. *Biophotonics Intl.*, **11**, 36–42.
26. Dame,R.T., van Marmeren,J., Luijsterburg,M.S., Mysiak,M.E., Janicijevic,A., Pazdzior,G., van der Vliet,P.C., Wyman,C. and Wuite,G.J.L. (2005) Analysis of scanning force microscopy images of protein-induced DNA bending using simulations. *Nucleic Acids Res.*, **33**, e68; erratum (2005). *Nucleic Acids Res.*, **33**, 2767.
27. Rivetti,C., Guthold,M. and Bustamante,C. (1999) Wrapping of DNA around the *E. coli* RNA polymerase open promoter complex. *EMBO J.*, **18**, 4464–4475.
28. Rivetti,C., Guthold,M. and Bustamante,C. (1996) Scanning force microscopy of DNA deposited onto mica: equilibration versus kinetic trapping studied by statistical polymer chain analysis. *J. Mol. Biol.*, **264**, 919–932.
29. Heddle,J.G., Mitelheiser,S., Maxwell,A. and Thomson,N.H. (2004) *J. Mol. Biol.*, **337**, 597–610.
30. Jafri,S., Chen,S. and Calvo,J.M. (1999) An Lrp-type transcriptional regulator from *Agrobacterium tumefaciens* condenses more than 100 nucleotides of DNA into globular nucleoprotein complexes. *J. Bacteriol.*, **184**, 5293–5300.
31. Peeters,E., Willaert,R., Maes,D. and Charlier,D. (2006) Ss-LrpB from *Sulfolobus solfataricus* condenses about 100 base pairs of its own operator DNA into globular nucleoprotein complexes. *J. Biol. Chem.*, **281**, 11721–11728.
32. Wyman,C., Rombel,I., North,A.K., Bustamante,C. and Kustu,S. (1997) Unusual oligomerization required for activity of NtrC, a bacterial enhancer-binding protein. *Science*, **275**, 1658–1661.
33. Ratcliff,G.C. and Erie,D.A. (2001) A novel single-molecule study to determine protein-protein association constants. *J. Am. Chem. Soc.*, **123**, 5632–5635.
34. Xue,Y., Ratcliff,G.C., Wang,H., Davis-Searles,P.R., Gray,M.D., Erie,D.A. and Redinbo,M.R. (2002) A minimal exonuclease domain of WRN forms a hexamer on DNA and possesses both 3′-5′ exonuclease and 5′-protruding strand endonuclease activities. *Biochemistry*, **41**, 2901–2912.
35. Beerens,N., Hoeijmakers,J.H.J., Kanaar,R., Vermeulen,W. and Wyman,C. (2005) The CSB protein actively wraps DNA. *J. Biol. Chem.*, **280**, 4722–4729.
36. Beloin,C., Jeusset,J., Révet,B., Mirambeau,G., Le Hégarat,F. and Le Cam,E. (2003) Contribution of DNA conformation and topology in right-handed DNA wrapping by the *Bacillus subtilis* LrpC protein. *J. Biol. Chem.*, **278**, 5333–5342.
37. Han,X. and Turnbough,C.L. Jr. (1998) Regulation of *carAB* expression in *Escherichia coli* occurs in part through UTP-sensitive reiterative transcription. *J. Bacteriol.*, **180**, 705–713.
38. Bouvier,J., Patte,J.C. and Stragier,P. (1984) Multiple regulatory signals in the control of the *Escherichia coli carAB* operon. *Proc. Natl Acad. Sci. USA*, **81**, 4139–4143.
39. Briozzo,P., Evrin,C., Meyer,P., Assairi,L., Joly,N, Bârzu,O. and Gilles,A.M. (2005) Structure of *Escherichia coli* UMP kinase differs from that of other NMP kinases and sheds new light on enzyme regulation. *J. Biol. Chem.*, **280**, 25533–25540.
40. Marco-Marín,C., Gil-Otiz,F. and Rubio,V. (2005) The crystal structure of *Pyrococcus furiosus* UMP kinase provides insights into catalysis and regulation in microbial nucleotide biosynthesis. *J. Mol. Biol.*, **352**, 438–454.
41. Vanhooff,V., Galloy,C., Agaisse,H., Lereclus,D., Révet,B. and Hallet,B. (2006) Self-control in DNA site-specific recombination mediated by the tyrosine recombinase TnpI. *Mol. Microbiol.*, **60**, 617–629.